

# Clinical Translation of a Dual Integrin $\alpha_v\beta_3$ - and Gastrin-Releasing Peptide Receptor-Targeting PET Radiotracer, $^{68}\text{Ga}$ -BBN-RGD

Jingjing Zhang<sup>1,2</sup>, Gang Niu<sup>2</sup>, Lixin Lang<sup>2</sup>, Fang Li<sup>1</sup>, Xinrong Fan<sup>3</sup>, Xuefeng Yan<sup>2</sup>, Shaobo Yao<sup>1</sup>, Weigang Yan<sup>3</sup>, Li Huo<sup>1</sup>, Libo Chen<sup>1</sup>, Zhiyuan Li<sup>4</sup>, Zhaohui Zhu<sup>1</sup>, and Xiaoyuan Chen<sup>2</sup>

<sup>1</sup>Department of Nuclear Medicine, Peking Union Medical College Hospital, Chinese Academy of Medical Sciences and Peking Union Medical College, Beijing, China; <sup>2</sup>Laboratory of Molecular Imaging and Nanomedicine (LOMIN), National Institute of Biomedical Imaging and Bioengineering (NIBIB), National Institutes of Health (NIH), Bethesda, Maryland; <sup>3</sup>Department of Urology, Peking Union Medical College Hospital, Chinese Academy of Medical Sciences and Peking Union Medical College, Beijing, China; and <sup>4</sup>Department of Pathology, Peking Union Medical College Hospital, Chinese Academy of Medical Sciences and Peking Union Medical College, Beijing, China

This study aimed to document the first-in-human application of a  $^{68}\text{Ga}$ -labeled heterodimeric peptide BBN-RGD (bombesin-RGD) that targets both integrin  $\alpha_v\beta_3$  and gastrin-releasing peptide receptor (GRPR). We evaluated the safety and assessed the clinical diagnostic value of  $^{68}\text{Ga}$ -BBN-RGD PET/CT in prostate cancer patients in comparison with  $^{68}\text{Ga}$ -BBN. **Methods:** Five healthy volunteers (4 men and 1 woman; age range, 28–53 y) were enrolled to validate the safety of  $^{68}\text{Ga}$ -BBN-RGD. Dosimetry was calculated using the OLINDA/EXM software. Thirteen patients with prostate cancer (4 newly diagnosed and 9 post-therapy) were enrolled. All the patients underwent PET/CT scans 15–30 min after intravenous injection of 1.85 MBq (0.05 mCi) per kilogram of body weight of  $^{68}\text{Ga}$ -BBN-RGD and also accepted  $^{68}\text{Ga}$ -BBN PET/CT within 2 wk for comparison. **Results:** With a mean injected dose of  $107.3 \pm 14.8$  MBq per patient, no side effect was found during the whole procedure and 2 wk follow-up, demonstrating the safety of  $^{68}\text{Ga}$ -BBN-RGD. A patient would be exposed to a radiation dose of 2.90 mSv with an injected dose of 129.5 MBq (3.5 mCi), which is much lower than the dose limit set by the Food and Drug Administration. In 13 patients with prostate cancer diagnosed by biopsy,  $^{68}\text{Ga}$ -BBN-RGD PET/CT detected 3 of 4 primary tumors, 14 metastatic lymph nodes, and 20 bone lesions with an  $\text{SUV}_{\text{max}}$  of  $4.46 \pm 0.50$ ,  $6.26 \pm 2.95$ , and  $4.84 \pm 1.57$ , respectively. Only 2 of 4 primary tumors, 5 lymph nodes, and 12 bone lesions were positive on  $^{68}\text{Ga}$ -BBN PET/CT, with the  $\text{SUV}_{\text{max}}$  of  $2.98 \pm 1.24$ ,  $4.17 \pm 1.89$ , and  $3.61 \pm 1.85$ , respectively. **Conclusion:** This study indicates the safety and efficiency of a new type of dual integrin  $\alpha_v\beta_3$ - and GRPR-targeting PET radiotracer in prostate cancer diagnosis and staging.

**Key Words:** BBN-RGD; PET; first-in-human; integrin  $\alpha_v\beta_3$ ; GRPR; prostate cancer

**J Nucl Med 2017; 58:228–234**

DOI: 10.2967/jnumed.116.177048

**P**rostate cancer is the second most frequently diagnosed cancer in men and the fifth leading cause of death worldwide (1). Accurate diagnosis and staging of prostate cancer is of topmost importance for effective therapy, especially at the early stage (2). Currently, the only definitive way to confirm prostate cancer is through prostate biopsy (3). However, prostate biopsy is usually deemed necessary by considering several factors including family history, race, abnormal lumps within the prostate, and an elevated serum prostate-specific antigen level. MRI is one of the major modalities for image-guided diagnosis, but a certain portion of prostate cancer lesions might still be missed using MRI (4). In these patients, PET imaging with probes targeting to various prostate cancer-specific markers will provide additional molecular information to facilitate lesion detection and staging (2).

Gastrin-releasing peptide receptor (GRPR) is an important biomarker used for prostate cancer diagnosis (5). Various GRPR-targeted imaging probes have been developed for noninvasive imaging of GRPR expression (6–8). Bombesin (BBN), an amphibian homolog of mammalian gastrin-releasing peptide (GRP), has been extensively used for imaging GRPR, after being labeled with various radionuclides (6,7,9–12). Several bombesin-related tracers have also been translated into the clinic for early phase studies (13–17). Previously, we have applied the GRPR-specific PET tracer  $^{68}\text{Ga}$ -NOTA-Aca-BBN(7-14) (denoted as  $^{68}\text{Ga}$ -BBN) for first-in-human studies in both healthy volunteers and patients with both low- and high-grade gliomas (18).

It has been found that both GRPR and integrin  $\alpha_v\beta_3$  are overexpressed in neoplastic cells of human prostate cancer (19). To target both receptors, a heterodimeric peptide BBN-RGD was synthesized from bombesin(7-14) and c(RGDyK) through a glutamate linker and then labeled with  $^{18}\text{F}$  (20). Within this heterodimer, the RGD moiety binds to integrin  $\alpha_v\beta_3$  receptor, which plays an important role in the regulation of tumor growth, angiogenesis, local invasiveness, and metastatic potential (21). In a PC3 xenograft model,  $^{18}\text{F}$ -FB-BBN-RGD had significantly higher tumor uptake

Received Apr. 18, 2016; revision accepted Jul. 26, 2016.

For correspondence or reprints contact either of the following: Fang Li, Department of Nuclear Medicine, Peking Union Medical College Hospital, Chinese Academy of Medical Sciences, Beijing 100730, China.

E-mail: lifang@pumch.cn

Xiaoyuan Chen, National Institutes of Health, 35A Convent Dr., GD937, Bethesda, MD 20892.

E-mail: shawn.chen@nih.gov

Published online Aug. 4, 2016.

COPYRIGHT © 2017 by the Society of Nuclear Medicine and Molecular Imaging.

than monomeric RGD and monomeric BBN peptide tracer analogs at all time points examined (20). A series of preclinical studies using the same strategy have confirmed several advantages of heterodimers including increased number of effective receptors, improved binding affinity, and pharmacokinetics (20,22–24).

In this study, for the first time, we translated BBN-RGD heterodimer into the clinic for the first-in-human study. The safety and dosimetry of  $^{68}\text{Ga}$ -BBN-RGD were evaluated in healthy volunteers. The preliminary diagnostic value of  $^{68}\text{Ga}$ -BBN-RGD PET/CT was also assessed in patients with primary or metastatic prostate cancer.

## MATERIALS AND METHODS

### Radiopharmaceutical Preparation

The macrocyclic chelator 1,4,7-triazacyclononane-*N,N',N''*-triacetic acid (NOTA)-conjugated BBN-RGD was synthesized according to a method described in our previous publication (22).  $^{68}\text{Ga}$  was eluted from a  $^{68}\text{Ge}/^{68}\text{Ga}$  generator (ITG) using 0.05 M HCl and mixed with 1.25 M NaOAc buffer to adjust pH to 4.0. Radiolabeling of BBN-RGD was performed in a sterile hot cell. The radiochemical purity of the product  $^{68}\text{Ga}$ -BBN-RGD exceeded 97%.  $^{68}\text{Ga}$ -BBN was synthesized following a procedure reported previously (18).

### Subject Enrollment

This clinical study was approved by the Institutional Review Board of Peking Union Medical College Hospital, Chinese Academy of Medical Sciences and Peking Union Medical College. All subjects signed a written informed consent form. Five healthy volunteers (4 men and 1 woman; mean age  $\pm$  SD, 45.2  $\pm$  9.9 y; age range, 28–53 y; mean weight  $\pm$  SD, 66.6  $\pm$  8.3 kg; weight range, 55–74 kg) were included in the study. Exclusion criteria consisted of conditions of mental illness, severe liver or kidney disease with serum creatinine greater than 3.0 mg/dL (270  $\mu\text{M}$ ), or any hepatic enzyme level 5 times or more than normal upper limit. Participants were also excluded if they were known to have severe allergy or hypersensitivity to intravenous radiographic contrast or claustrophobia during PET/CT scanning or if they were pregnant or breast-feeding.

A total of 13 patients with prostate cancer (age range, 49–70 y; mean age, 62.4  $\pm$  6.0 y), of which 4 patients were newly diagnosed as having prostate cancer by sextant core-needle biopsy and had not received any prior therapy and 9 patients underwent prostatectomy or brachytherapy, were enrolled with written informed consent. The inclusion criteria were being between 40 and 80 y old, having a prostate neoplasm identified by ultrasound or MRI, being diagnosed by needle biopsy as having prostate cancer, having undergone whole-body bone scanning, and being able to provide basic information and sign the written informed consent form. The exclusion criteria included claustrophobia, kidney or liver failure, and inability to fulfill the study. The demographics of the patients are listed in Table 1.

$^{68}\text{Ga}$ -BBN-RGD PET/CT,  $^{68}\text{Ga}$ -BBN PET/CT, MRI, and methylene diphosphonate (MDP) bone scanning were performed within 2 wk for comparison. All the 4 newly diagnosed prostate cancer patients underwent radical prostatectomy surgery within 1 wk after  $^{68}\text{Ga}$ -BBN-RGD PET/CT. The existence of malignancy in the prostate gland and lymph nodes was confirmed by histologic examination with postoperation sampling or biopsy. The examination was determined by 2 pathologists independently, with a third pathologist used to reach consensus if there were any discrepancies.

### Examination Procedures

For healthy volunteers, the blood pressure, pulse, respiratory frequency, and temperature were measured, and routine blood and urine tests, liver function, and renal function were examined immediately

before and 24 h after the scan. In addition, any possible side effects during  $^{68}\text{Ga}$ -BBN-RGD PET/CT scanning and within 1 wk after the examination were collected and analyzed as safety data.

No specific subject preparation was requested on the day of  $^{68}\text{Ga}$ -BBN-RGD PET/CT scanning. For the volunteers, after the whole-body low-dose CT scan, nearly 111–148 MBq (3–4 mCi) of  $^{68}\text{Ga}$ -BBN-RGD were injected intravenously, followed by serial whole-body dynamic PET acquisitions. The whole body (from the top of skull to the middle of femur) of each volunteer was covered by 6 bed positions. The acquisition duration was 20 s/bed position at 1 min after injection; 40 s/bed position at 5, 10, and 15 min after injection; and 2 min/bed position at 30, 45, and 60 min after injection.

For the patients,  $^{68}\text{Ga}$ -BBN-RGD PET/CT scanning was performed at 15–30 min after tracer administration. For each patient, 1.85 MBq (0.05 mCi) of  $^{68}\text{Ga}$ -BBN-RGD per kilogram of body weight were injected intravenously. After a low-dose CT scan, whole-body PET was performed with 2 min per bed position (5–6 bed positions depending on the height of the patient). The emission data were corrected for randoms, dead time, scattering, and attenuation. The conventional reconstruction algorithm was used, and the images were zoomed with a factor of 1.2. The images were transferred to a MMWP workstation (Siemens) for analysis.

In all patients, a second scan using  $^{68}\text{Ga}$ -BBN was obtained within 2 wk for comparison. For each patient, 1.85 MBq (0.05 mCi) of  $^{68}\text{Ga}$ -BBN per kilogram of body weight were injected intravenously. The imaging procedure and data analysis are the same as those for  $^{68}\text{Ga}$ -BBN-RGD PET/CT. MRI was performed with a standard clinical procedure.

### Image and Data Analysis

A Siemens MMWP workstation was used for postprocessing. Visual analysis was used to determine the general biodistribution and the temporal and intersubject stability. The volume of interest of normal organs/tissues and concerned lesions were drawn on the serial images. The radioactivity concentration and SUV in the volumes of interest were obtained through the software.

For the volunteers, the dosimetry calculation was performed according to the EANM Dosimetry Guidance (25) and calculated using OLINDA/EXM (version 1.1; Vanderbilt University) with the procedure reported in a previous study (18). The void time of the bladder was set as 60 min. The absorbed doses were calculated by entering the time-integrated activity coefficient for all source organs into OLINDA/EXM for either a 73.7-kg adult man or a 56.9-kg adult woman.

For the patients, regions of interest were drawn manually on the site of lesions using a 3-dimensional ellipsoid isocontour on each image with the assistance of the corresponding CT images by 2 experienced nuclear medical physicians. The results were expressed as  $\text{SUV}_{\text{mean}}$  and  $\text{SUV}_{\text{max}}$ .

### $^{99\text{m}}\text{Tc}$ -MDP Bone Scanning

For the patients, bone scan images were obtained using a dual-head Siemens SPECT scanner. Planar images of the whole-body skeleton were acquired in the anterior and posterior views 3 h after intravenous injection of 925 MBq (25 mCi) of  $^{99\text{m}}\text{Tc}$ -MDP.

### Immunohistochemical Staining

Representative tumor and lymph node samples were fixed with 10% neutral buffered formalin and embedded in paraffin. After blocking and washing, 5- $\mu\text{m}$ -thick tissue sections were incubated with mouse antihuman monoclonal antibody against human GRPR (PA5-256791; Thermo Fisher Scientific) and integrin  $\alpha_v\beta_3$  (1:200, sc-7312; Santa Cruz Biotechnology), respectively. Six fields were randomly selected from each section and observed using a light microscope (BX41; Olympus). For semiquantification of GRPR and integrin  $\alpha_v\beta_3$  expression, 5 entire high-power fields ( $\times 40$ ) containing clusters of malignant cells

**TABLE 1**  
Patient Demographics

Patient no.	Age (y)	PSA (ng/mL)	GS	Treatment	Bone scan	MRI	<sup>68</sup> Ga-BBN-RGD PET/CT	<sup>68</sup> Ga-BBN PET/CT
1	69	109.1	7	RP	(-)	PT	PT	PT
2	61	7.31	7	RP	(-)	PT	PT	PT
3	55	30.3	9	RP	(-)	PT	(-)	(-)
4	68	25.59	7	RP	(+)	PT/LNs/BM	PT/LNs/BM	LNs
5	64	36.1	7	BT + ADT	(-)	(-)	BM	BM
6	78	108.1	7	RP + RT + C	(+)	BM	BM	(-)
7	67	5.34	6	RT + ADT	(-)	(-)	(-)	(-)
8	62	20.2	8	ADT	(+/-)	BM	BM	BM
9	79	15.79	8	BT + C	(+)	LNs/BM	LNs/BM	BM
10	59	5.78	8	RP + RT	(+/-)	BM	BM	BM
11	58	4.15	7	RP	(+/-)	(-)	(-)	(-)
12	70	105	7	BT + C	(+)	(-)	BM	(-)
13	65	4.1	9	RP + RT	(-)	LNs	LNs	(-)

PSA = prostate-specific antigen; GS = Gleason score; RP = radical prostatectomy; PT = primary tumor; LNs = lymph nodes involvement; BM = bone metastasis; BT = brachytherapy; ADT = androgen-deprivation therapy; RT = radiation therapy; C = chemotherapy.

were identified randomly per slide and scored for intensity and percentage of GRPR and integrin  $\alpha_v\beta_3$  staining expression. The procedure was repeated by 2 independent experienced examiners.

## RESULTS

### Safety

No adverse events or serious adverse events occurred after <sup>68</sup>Ga-BBN-RGD injection for all the healthy volunteers and the patients, and no obvious changes in vital signs or clinical laboratory

tests were found before and after the injection of <sup>68</sup>Ga-BBN-RGD. For the patients, 1.85 MBq (0.05 mCi) of <sup>68</sup>Ga-BBN-RGD per kilogram of body weight were injected intravenously. The median and maximum injected dose was  $123.7 \pm 11.5$  MBq and 146.2 MBq, respectively. The median and maximum injected mass was  $12.3 \pm 2.6$   $\mu$ g and 15  $\mu$ g, respectively.

### Biodistribution and Dosimetry

After intravenous administration, <sup>68</sup>Ga-BBN-RGD showed rapid clearance through the kidneys with  $49.9\% \pm 10.2\%$  of total injected radioactivity observed in the urine at 30 min after injection. The pancreas also had high accumulation, with an  $SUV_{mean}$  of  $10.96 \pm 1.10$  at 30 min after injection, which is in the line with the known high-level expression of GRPR in the pancreas (26). The liver and spleen showed moderate uptake, with an  $SUV_{mean}$  of  $1.54 \pm 0.24$  and  $1.80 \pm 0.46$ , respectively. Low background activities in the brain, lung, and muscle were found with SUVs of  $0.16 \pm 0.05$ ,  $0.44 \pm 0.11$ , and  $0.40 \pm 0.16$ , respectively (Supplemental Table 1 [supplemental materials are available at <http://jnm.snmjournals.org>]; Fig. 1).

The estimated absorbed dose of <sup>68</sup>Ga-BBN-RGD for each organ derived from PET/CT images of healthy volunteers is shown in Table 2. Because of the high accumulation of radioactivity in the urinary bladder, the urinary bladder wall had the highest absorbed dose of  $0.33 \pm 0.16$  mSv/MBq, which was followed by the kidneys ( $0.0647 \pm 0.0436$  mSv/MBq) and pancreas

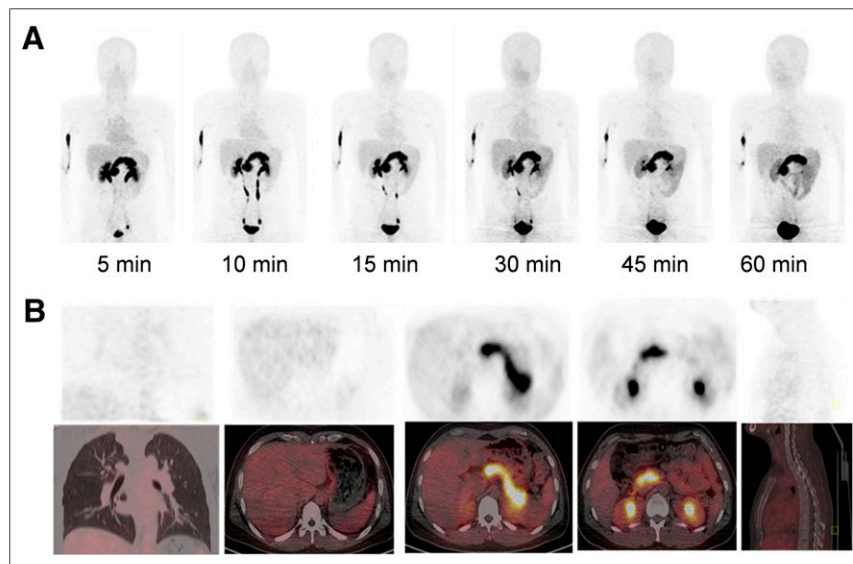


**FIGURE 1.** (A) Multiple-time-point whole-body maximum-intensity-projection PET images at 5, 10, 15, 30, 45, and 60 min after intravenous administration of <sup>68</sup>Ga-BBN-RGD in 47-y-old male volunteer. (B) PET/CT showed tracer uptake in major organs at 30 min after intravenous administration of 129.5 MBq (3.5 mCi) of <sup>68</sup>Ga-BBN-RGD to a male volunteer.

**TABLE 2**

Estimated Absorbed Dose After Intravenous Administration of  $^{68}\text{Ga}$ -BBN-RGD (mSv/MBq;  $n = 5$ ; 4 Men and 1 Woman)

Target organ	Mean	SD
Adrenals	4.70E-03	1.45E-03
Brain	1.32E-03	1.80E-04
Breasts	2.50E-03	1.00E-03
Gallbladder wall	4.88E-03	1.25E-03
Lower large intestine wall	7.16E-03	1.71E-03
Small intestine	5.02E-03	1.38E-03
Stomach wall	3.95E-03	1.18E-03
Upper large intestine wall	4.70E-03	1.36E-03
Heart wall	8.38E-03	2.31E-03
Kidneys	6.47E-02	4.36E-02
Liver	1.55E-02	6.11E-03
Lungs	3.88E-03	8.39E-04
Muscle	4.48E-03	1.09E-03
Ovaries	6.97E-03	1.70E-03
Pancreas	5.23E-02	1.73E-02
Red marrow	4.89E-03	7.66E-04
Osteogenic cells	5.32E-03	1.58E-03
Skin	2.64E-03	9.64E-04
Spleen	1.14E-02	4.25E-03
Testes	4.85E-03	1.04E-03
Thymus	2.90E-03	1.01E-03
Thyroid	2.67E-03	9.75E-04
Urinary bladder wall	3.33E-01	1.60E-01
Uterus	1.55E-02	
Total body	5.43E-03	1.56E-03
Effective dose equivalent	3.21E-02	1.38E-02
Effective dose	2.23E-02	9.26E-03

( $0.0523 \pm 0.0173$  mSv/MBq). The total effective dose equivalent and effective dose were  $0.0321 \pm 0.0138$  and  $0.0223 \pm 0.0093$  mSv/MBq, respectively.

#### Detection of Primary Prostate Cancer

For the 4 patients with primary prostate cancer,  $^{68}\text{Ga}$ -BBN-RGD PET/CT showed positive findings in 3 lesions (75%). The primary lesions were diagnosed by MRI, and the diagnosis was confirmed by needle biopsy. The  $\text{SUV}_{\text{mean}}$  and  $\text{SUV}_{\text{max}}$  were  $3.26 \pm 0.52$  and  $4.46 \pm 0.50$ , respectively. Two of the 4 lesions were positive on  $^{68}\text{Ga}$ -BBN PET/CT, with the average mean and maximum SUVs of 2.09 and 2.98, respectively (Fig. 2). To further elucidate the findings from PET, we performed immunohistochemical staining against GRPR and integrin  $\alpha_v\beta_3$  with the biopsy samples. As shown in Figure 3, both GRPR- and integrin-positive staining were found in 2 patients, GRPR-negative and integrin  $\alpha_v\beta_3$ -positive staining in 1 patient, and both GRPR- and  $\alpha_v\beta_3$ -negative staining in 1 patient.

#### Detection of Lymph Node and Bone Metastasis

For all the 13 patients with prostate cancer,  $^{68}\text{Ga}$ -BBN-RGD PET/CT detected 14 metastatic lymph nodes and 20 bone lesions.

The average and maximum SUVs of all the lymph node metastatic lesions were  $3.77 \pm 1.65$  and  $6.26 \pm 2.95$  at 30 min after injection, respectively. The average and maximum SUVs of all the bone lesions were  $3.01 \pm 0.84$  and  $4.84 \pm 1.57$  at 30 min after injection, respectively. Only 5 lymph node metastases and 12 bone lesions were detected by  $^{68}\text{Ga}$ -BBN PET/CT, with significantly lower average and maximum SUVs ( $2.79 \pm 1.19$  and  $4.17 \pm 1.89$  for lymph nodes and  $2.26 \pm 1.15$  and  $3.61 \pm 1.85$  for bone lesions at 30 min after injection,  $P < 0.05$ ) (Figs. 3 and 4).

In comparison, MRI detected all the 14 lymph nodes in the pelvic cavity. However, only 5 bone lesions located in the ilium, pubis, rib, and thoracic and lumbar vertebrae were detected by MRI. Eleven of 20 lesions identified by  $^{68}\text{Ga}$ -BBN-RGD PET/CT showed positive signal with MDP bone scanning. Besides these 20 lesions, 14 abnormal hotspots were shown on MDP SPECT bone scanning. These hotspots were confirmed as benign lesions by MRI and history such as traumatic fracture, vertebral degeneration, and spinal stenosis (Fig. 5).

#### DISCUSSION

$^{68}\text{Ga}$ -BBN-RGD was found to be safe and well tolerated in all healthy volunteers and recruited patients, with no adverse events occurring after tracer injection. With a typical 130 MBq (3.5 mCi) injected activity of  $^{68}\text{Ga}$ -BBN, the whole-body effective dose is 2.90 mSv, which is much lower than the dose limit set by the Food and Drug Administration (27). All these data confirmed the safety of  $^{68}\text{Ga}$ -BBN for further clinical applications.

One major advantage of heterodimer over the corresponding monomers is the multivalency effect, resulting in improved binding affinity and increased number of effective receptors (20,22–24). Consistently, both  $^{68}\text{Ga}$ -BBN-RGD and  $^{68}\text{Ga}$ -BBN showed uptake in the primary prostate tumors that were either

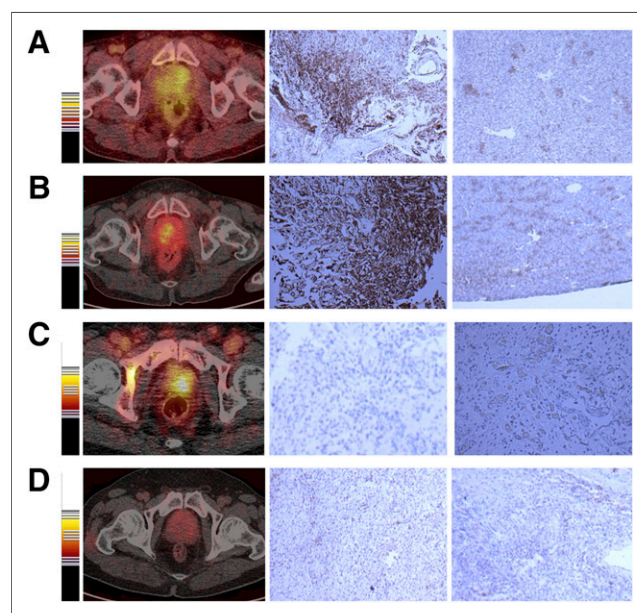


**FIGURE 2.**  $^{68}\text{Ga}$ -BBN-RGD PET/CT of primary tumors of 4 prostate cancer patients. Immunohistologic staining against GRPR and integrin  $\alpha_v\beta_3$  was performed with biopsy samples. (A and B) GRPR-positive and  $\alpha_v\beta_3$ -positive. (C) GRPR-negative and  $\alpha_v\beta_3$ -positive. (D) GRPR-negative and  $\alpha_v\beta_3$ -negative.

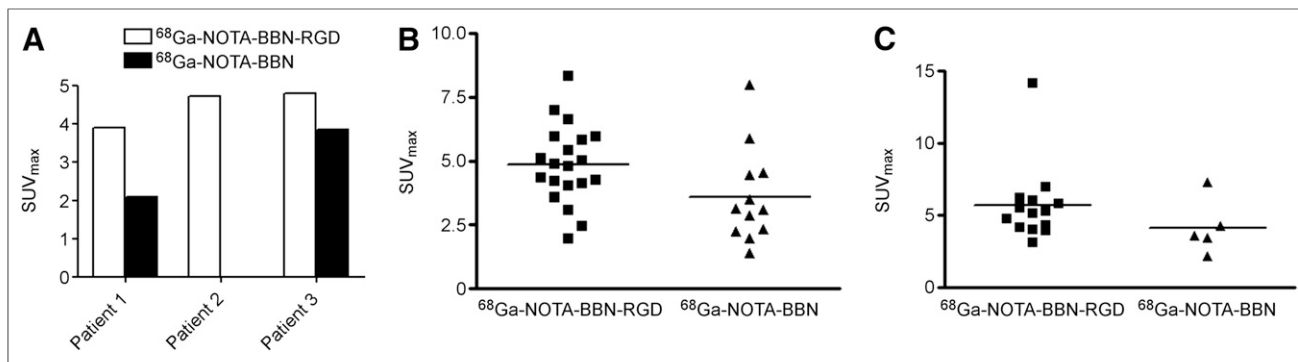


**FIGURE 3.** Quantitative comparison between <sup>68</sup>Ga-BBN-RGD PET/CT and <sup>68</sup>Ga-BBN PET/CT in primary tumor (A), bone metastases (B), and lymph node metastases (C).

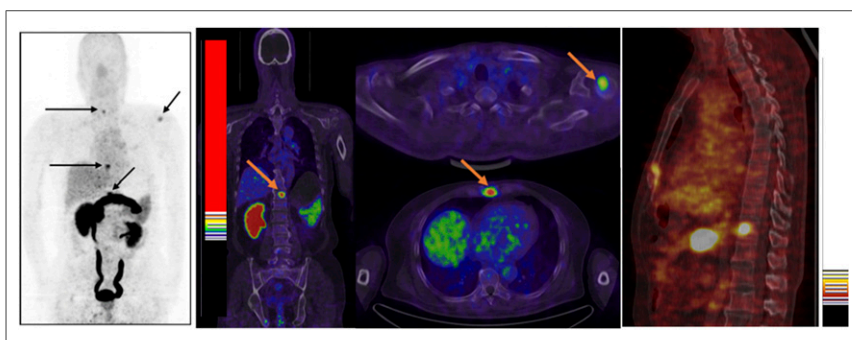


**FIGURE 4.** <sup>68</sup>Ga-BBN PET/CT of a 64-y-old man newly diagnosed as having prostate cancer by biopsy. Multiple bone metastatic lesions (arrow) were detected.

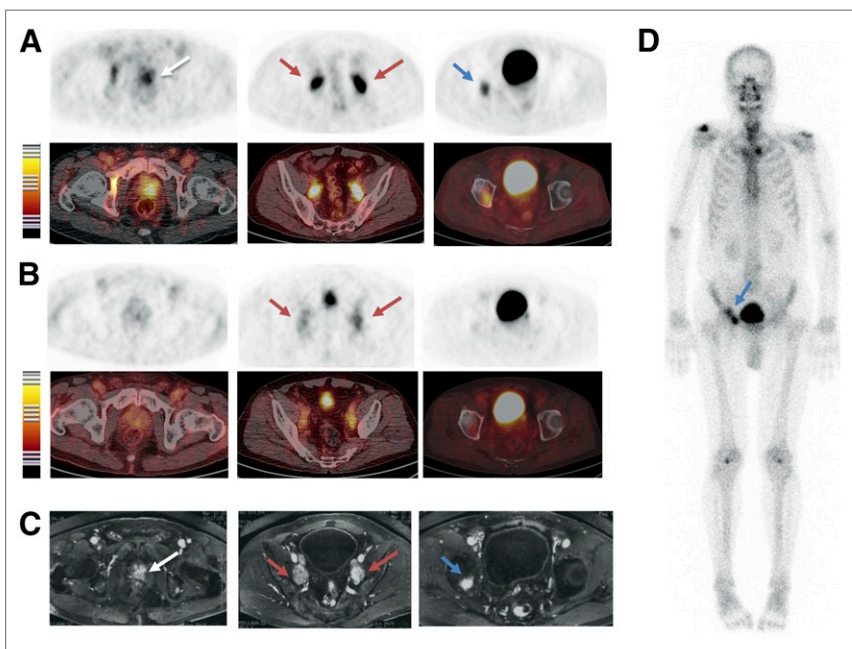


**FIGURE 5.** Comparison of <sup>68</sup>Ga-BBN-RGD PET/CT (A), <sup>68</sup>Ga-BBN PET/CT (B), MRI (C), and <sup>99m</sup>Tc-MDP bone scan (D) in a 63-y-old man diagnosed as having prostate cancer (white arrow) with lymph node involvement (red arrow) and bone metastasis (blue arrow) before prostatectomy. Both <sup>68</sup>Ga-BBN-RGD PET/CT and MRI detected primary tumors, multiple lymph node involvement, and bone metastatic lesion, whereas <sup>68</sup>Ga-BBN PET/CT detected only lymph node metastases.

GPRR-positive or integrin  $\alpha_v\beta_3$ -positive. However, <sup>68</sup>Ga-BBN failed to visualize the lesions that were GPRR-negative and integrin  $\alpha_v\beta_3$ -positive whereas <sup>68</sup>Ga-BBN-RGD showed positive results in these cases. It is also reasonable that both tracers had negative results in the lesion with neither GRPR nor integrin  $\alpha_v\beta_3$  overexpression, implying that <sup>68</sup>Ga-BBN-RGD PET/CT is specific for GRPR and integrin  $\alpha_v\beta_3$ . Because of the limited size of the patient population, the frequency of prostate cancer tumors both GRPR-negative and integrin  $\alpha_v\beta_3$ -negative cannot be determined in this study and will need further investigation. With a receptor binding assay in specimens of primary prostate cancer, 37% of samples showed negative bombesin binding (28). Thus, it is foreseeable that <sup>68</sup>Ga-BBN-RGD PET will increase the detection rate of primary prostate cancer.

About 40%–60% of men with prostate cancer have lymph node involvement or extracapsular disease at the time of presentation, and 70% develop lymph node metastasis during the course (29). Although treatable at the early stage, prostate cancer is prone to metastasis; an effective and specific imaging method of detecting both primary and metastatic lesions is thus of critical importance to manage patients with prostate cancer. In 3 patients with LN metastasis, <sup>68</sup>Ga-BBN-RGD PET/CT identified all 14 metastasized LNs as MRI did, which is dramatically better than <sup>68</sup>Ga-BBN PET/CT. In addition, the average SUV of <sup>68</sup>Ga-BBN-RGD PET/CT is significantly higher than that of <sup>68</sup>Ga-BBN PET/CT. Durkan et al. (30) proposed that prostate cancer cells differentially express specific receptors depending on factors such as chronicity and metastatic nature. Thus, compounds capable of targeting more than one biomarker would have the ability of

binding to both early and metastatic stages of prostate cancer, creating the possibility for a more prompt and accurate diagnostic profile for both the primary and the metastatic tumors. This may partially explain our results that  $^{68}\text{Ga}$ -BBN-RGD PET/CT is better than  $^{68}\text{Ga}$ -BBN PET/CT in detecting metastasized LNs.

Autopsy studies suggest that approximately 80%–90% of prostate cancer patients have bone metastasis at death although only 6% of men with prostate cancer have metastatic disease at diagnosis (31). Skeletal metastasis of prostate cancer is routinely assessed by  $^{99\text{m}}\text{Tc}$ -MDP bone scanning for the staging of prostate cancer.  $^{99\text{m}}\text{Tc}$ -MDP bone scanning is sensitive but lacks specificity because localized skeletal accumulation of  $^{99\text{m}}\text{Tc}$ -MDP can be observed in the case of trauma and infection. Thus,  $^{99\text{m}}\text{Tc}$ -MDP bone scanning may not be recommended in asymptomatic patients if the serum prostate-specific antigen level is less than 20 ng/mL in the presence of well-differentiated or moderately differentiated tumors (3). In this study,  $^{68}\text{Ga}$ -BBN-RGD PET/CT detected 20 bone lesions in 7 patients either with primary prostate cancer or after radical prostatectomy. Eleven of these 20 lesions showed positive signal on  $^{99\text{m}}\text{Tc}$ -MDP bone scanning, and only 5 of these lesions were detectable with MRI. More importantly, the patients with bone metastases do not necessarily have an elevated prostate-specific antigen level (Table 1).

Bisanz et al. (32) have illustrated a positive role of  $\alpha_v$  integrins on prostate tumor survival in the bone. Integrin  $\alpha_v\beta_3$  activation on tumor cells is essential for the recognition of key bone-specific matrix proteins, suggesting that the  $\alpha_v\beta_3$  integrin modulates prostate cancer growth in distant metastasis (33). In a recently published clinical study in prostate cancer patients using  $^{18}\text{F}$ -galacto-RGD PET, 58 of 74 bone lesions were identified, with a detection rate of 78.4% (34). Thus, RGD moiety in  $^{68}\text{Ga}$ -BBN-RGD may play a major role in bone metastasis detection. However, 1 limitation of this study is the lack of histologic confirmation of the detected bone metastasis. Thus, the GRPR and integrin  $\alpha_v\beta_3$  expression status in these metastases are unknown. In addition, the accurate diagnostic and prognostic value of  $^{68}\text{Ga}$ -BBN-RGD warrants further larger scale clinical investigations.

Besides BBN-based imaging probes, various PET tracers have been used for the detection of prostate cancer such as  $^{18}\text{F}$ -FDG,  $^{11}\text{C}$ -choline or  $^{18}\text{F}$ -fluorocholine,  $^{11}\text{C}$ -acetate,  $^{18}\text{F}$ -FACBC, and prostate-specific membrane antigen targeting agents (35). Each of these tracers has advantages and limitations because of the heterogeneity of the disease. We expect  $^{68}\text{Ga}$ -BBN-RGD to play an additive role in staging and detecting prostate cancer and provide guidance for internal radiation therapy using the same peptide labeled with therapeutic radionuclides.

## CONCLUSION

This study indicates the safety and the efficacy  $^{68}\text{Ga}$ -BBN-RGD, a heterodimeric PET tracer targeting both GRPR and integrin  $\alpha_v\beta_3$ .  $^{68}\text{Ga}$ -BBN-RGD PET/CT would have great value in discerning both primary prostate cancers and metastases in lymph nodes and skeleton, providing tumor staging information and monitoring response of bone metastases to therapy.

## DISCLOSURE

This work was supported by the Intramural Research Program (IRP) of the National Institute of Biomedical Imaging and Bioengineering (NIBIB), National Institutes of Health (NIH),

the National Natural Science Foundation of China projects (81171369, 81171370, and 81271614), and a Special Scientific Research Fund for Public Welfare of Healthcare in China (201402001). No other potential conflict of interest relevant to this article was reported.

## REFERENCES

1. Torre LA, Bray F, Siegel RL, Ferlay J, Lortet-Tieulent J, Jemal A. Global cancer statistics, 2012. *CA Cancer J Clin*. 2015;65:87–108.
2. Maurer T, Eiber M, Schwaiger M, Gschwend JE. Current use of PSMA-PET in prostate cancer management. *Nat Rev Urol*. 2016;13:226–235.
3. Heidenreich A, Bastian PJ, Bellmunt J, et al. EAU guidelines on prostate cancer: part 1—screening, diagnosis, and local treatment with curative intent: update 2013. *Eur Urol*. 2014;65:124–137.
4. Barentsz JO, Richenberg J, Clements R, et al. ESUR prostate MR guidelines 2012. *Eur Radiol*. 2012;22:746–757.
5. Ananias HJ, van den Heuvel MC, Helfrich W, de Jong IJ. Expression of the gastrin-releasing peptide receptor, the prostate stem cell antigen and the prostate-specific membrane antigen in lymph node and bone metastases of prostate cancer. *Prostate*. 2009;69:1101–1108.
6. Carlucci G, Kuipers A, Ananias H, et al. GRPR-selective PET imaging of prostate cancer using [ $^{18}\text{F}$ ]-lanthionine-bombesin analogs. *Peptides*. 2015;67:45–54.
7. Chen X, Park R, Hou Y, et al. microPET and autoradiographic imaging of GRP receptor expression with  $^{64}\text{Cu}$ -DOTA-[Lys $^3$ ]bombesin in human prostate adenocarcinoma xenografts. *J Nucl Med*. 2004;45:1390–1397.
8. Garrison JC, Rold TL, Sieckman GL, et al. In vivo evaluation and small-animal PET/CT of a prostate cancer mouse model using  $^{64}\text{Cu}$  bombesin analogs: side-by-side comparison of the CB-TE2A and DOTA chelation systems. *J Nucl Med*. 2007;48:1327–1337.
9. Smith CJ, Volkert WA, Hoffman TJ. Radiolabeled peptide conjugates for targeting of the bombesin receptor superfamily subtypes. *Nucl Med Biol*. 2005;32:733–740.
10. Prasanphanich AF, Nanda PK, Rold TL, et al. [ $^{64}\text{Cu}$ -NOTA-8-Aoc-BBN(7-14)NH $_2$ ] targeting vector for positron-emission tomography imaging of gastrin-releasing peptide receptor-expressing tissues. *Proc Natl Acad Sci USA*. 2007;104:12462–12467.
11. Mansi R, Wang X, Forrer F, et al. Development of a potent DOTA-conjugated bombesin antagonist for targeting GRPr-positive tumours. *Eur J Nucl Med Mol Imaging*. 2011;38:97–107.
12. Pourghasian M, Liu Z, Pan J, et al.  $^{18}\text{F}$ -AmBF 3-MJ9: A novel radiofluorinated bombesin derivative for prostate cancer imaging. *Bioorg Med Chem*. 2015;23:1500–1506.
13. Van de Wiele C, Dumont F, Dierckx RA, et al. Biodistribution and dosimetry of  $^{99\text{m}}\text{Tc}$ -RP527, a gastrin-releasing peptide (GRP) agonist for the visualization of GRP receptor-expressing malignancies. *J Nucl Med*. 2001;42:1722–1727.
14. Van de Wiele C, Phonteyne P, Pauwels P, et al. Gastrin-releasing peptide receptor imaging in human breast carcinoma versus immunohistochemistry. *J Nucl Med*. 2008;49:260–264.
15. Nock B, Maina T. Tetraamine-coupled peptides and resulting  $^{99\text{m}}\text{Tc}$ -radioligands: an effective route for receptor-targeted diagnostic imaging of human tumors. *Curr Top Med Chem*. 2012;12:2655–2667.
16. Ananias HJ, Yu Z, Dierckx RA, et al.  $^{99\text{m}}\text{Tc}$ -HYNIC (tricine/TPPTS)-Aca-bombesin (7-14) as a targeted imaging agent with microSPECT in a PC-3 prostate cancer xenograft model. *Mol Pharm*. 2011;8:1165–1173.
17. Ananias HJ, Yu Z, Hoving HD, et al. Application of  $^{99\text{m}}\text{Tc}$ -HYNIC (tricine/TPPTS)-aca-bombesin (7-14) SPECT/CT in prostate cancer patients: a first-in-man study. *Nucl Med Biol*. 2013;40:933–938.
18. Zhang J, Li D, Lang L, et al.  $^{68}\text{Ga}$ -NOTA-Aca-BBN(7-14) PET/CT in healthy volunteers and glioma patients. *J Nucl Med*. 2016;57:9–14.
19. Beer M, Montani M, Gerhardt J, et al. Profiling gastrin-releasing peptide receptor in prostate tissues: Clinical implications and molecular correlates. *Prostate*. 2012;72:318–325.
20. Li Z-B, Wu Z, Chen K, Ryu EK, Chen X.  $^{18}\text{F}$ -labeled BBN-RGD heterodimer for prostate cancer imaging. *J Nucl Med*. 2008;49:453–461.
21. Niu G, Chen X. Why integrin as a primary target for imaging and therapy. *Theranostics*. 2011;1:30–47.
22. Liu Z, Niu G, Wang F, Chen X.  $^{68}\text{Ga}$ -labeled NOTA-RGD-BBN peptide for dual integrin and GRPR-targeted tumor imaging. *Eur J Nucl Med Mol Imaging*. 2009;36:1483–1494.

23. Liu Z, Yan Y, Liu S, Wang F, Chen X.  $^{18}\text{F}$ ,  $^{64}\text{Cu}$ , and  $^{68}\text{Ga}$  labeled RGD-bombesin heterodimeric peptides for PET imaging of breast cancer. *Bioconjug Chem*. 2009;20:1016–1025.
24. Eder M, Schafer M, Bauder-Wust U, Haberkorn U, Eisenhut M, Kopka K. Pre-clinical evaluation of a bispecific low-molecular heterodimer targeting both PSMA and GRPR for improved PET imaging and therapy of prostate cancer. *Prostate*. 2014;74:659–668.
25. Lassmann M, Chiesa C, Flux G, Bardies M. EANM Dosimetry Committee guidance document: good practice of clinical dosimetry reporting. *Eur J Nucl Med Mol Imaging*. 2011;38:192–200.
26. Gonzalez N, Moody TW, Igarashi H, Ito T, Jensen RT. Bombesin-related peptides and their receptors: recent advances in their role in physiology and disease states. *Curr Opin Endocrinol Diabetes Obes*. 2008;15:58–64.
27. Mitra ES, Goris ML, Iagaru AH, et al. Pilot pharmacokinetic and dosimetric studies of  $^{18}\text{F}$ -FPPRGD2: a PET radiopharmaceutical agent for imaging  $\alpha\text{v}\beta\text{3}$  integrin levels. *Radiology*. 2011;260:182–191.
28. Sun B, Halmos G, Schally AV, Wang X, Martinez M. Presence of receptors for bombesin/gastrin-releasing peptide and mRNA for three receptor subtypes in human prostate cancers. *Prostate*. 2000;42:295–303.
29. Vag T, Heck MM, Beer AJ, et al. Preoperative lymph node staging in patients with primary prostate cancer: comparison and correlation of quantitative imaging parameters in diffusion-weighted imaging and  $^{11}\text{C}$ -choline PET/CT. *Eur Radiol*. 2014;24:1821–1826.
30. Durkan K, Jiang Z, Rold TL, et al. A heterodimeric [RGD-Glu- $^{64}\text{Cu}$ -NO $_2$ A]-6-Ahx-RM2] alphavbeta3/GRPr-targeting antagonist radiotracer for PET imaging of prostate tumors. *Nucl Med Biol*. 2014;41:133–139.
31. Bubendorf L, Schöpfer A, Wagner U, et al. Metastatic patterns of prostate cancer: an autopsy study of 1,589 patients. *Hum Pathol*. 2000;31:578–583.
32. Bisanz K, Yu J, Edlund M, et al. Targeting ECM–integrin interaction with liposome-encapsulated small interfering RNAs inhibits the growth of human prostate cancer in a bone xenograft imaging model. *Mol Ther*. 2005;12:634–643.
33. McCabe NP, De S, Vasanthi A, Brainard J, Byzova T. Prostate cancer specific integrin  $\alpha\text{v}\beta\text{3}$  modulates bone metastatic growth and tissue remodeling. *Oncogene*. 2007;26:6238–6243.
34. Beer AJ, Schwarzenbock SM, Zantl N, et al. Non-invasive assessment of inter- and inpatient variability of integrin expression in metastasized prostate cancer by PET. *Oncotarget*. 2016;7:28151–28159.
35. Kitajima K, Yamamoto S, Fukushima K, Minamimoto R, Kamai T, Jadvar H. Update on advances in molecular PET in urological oncology. *Jpn J Radiol*. 2016;34:470–485.